Quantum Effects on the Free Energy of Ionic Aqueous Clusters Evaluated by Nonequilibrium Computational Methods

Lisandro Hernández de la Peña*,† and Gilles H. Peslherbe

Centre for Research in Molecular Modeling and Department of Chemistry & Biochemistry, Concordia University, Montreal, Canada

Received: September 10, 2009; Revised Manuscript Received: February 17, 2010

Nonequilibrium simulation methods and rigid-body path-integral techniques are combined to estimate the relevance of protonic quantum effects in the free energy of ion−water clusters. The Crooks' fluctuation relation is used to quantitatively characterize the impact of quantum effects on the dissociation free energy of the paradigm $I^-(H_2O)_5$. By use of a rigorous smoothing procedure in the calculation of the work distributions, the effects are found to be about 11% and therefore non-negligible. Quantum effects on the potential of mean force of $Na^+(H_2O)_{12}$ were also evaluated using Jarzynski's work theorem for a reaction coordinate, and they were also found to be significant. The results suggest that quantization should play a significant role in the kinetics of ionic transport in aqueous environments.

I. Introduction

To gain insight into microsolvation processes, the structure and thermodynamics of ions in aqueous clusters have been the subject of many studies.[1–4] For instance, the formation enthalpy or free energy of ionic clusters yields significant information that can in turn be compared with available experimental data. While most theoretical estimates of the free energy to date have been obtained by standard equilibrium methods, recent progress in nonequilibrium statistical mechanics has provided a number of powerful (nonequilibrium) techniques for the computation of equilibrium properties.

Two particularly important relations in nonequilibrium statistical mechanics are the Jarzynski work identity[5,6] and the Crooks fluctuation relation.[7,8] They provide the basis for the calculation of free energy differences through irreversible processes by means of evaluating the work distribution along a dynamical trajectory with a time-evolving Hamiltonian. In Jarzynski's identity, the Hamiltonian evolves continuously from the one that defines the initial state to the one that defines the final state, and the exponential average of the work involved in the process yields the free energy difference between these two equilibrium states. In Crooks' relation, the intersection of the work distribution of the forward and reverse processes yields the free energy difference. Nonequilibrium techniques can also be used for the calculation of potentials of mean force[9–11] through the so-called single-molecule manipulation or *pulling* process.

Although the aforementioned relations were initially formulated for classical systems, they are also valid for quantum systems.[12–20] In fact, the identities mentioned above hold for the exact real-time quantum dynamics, as well as for the fictitious dynamics invoked in the path-integral representation of a quantum system.[19,20] In this context, it has been recently shown[19,20] that the mapping of a quantum system into an isomorphic classical field can be cast in a regularized form where the (fictitious) work distribution converges as the number of degrees of freedom goes to infinity. The artificial dynamics associated with the isomorphic classical field has the advantage of avoiding the well-known complications that arise in real-time quantum dynamics.

The nonequilibrium approach, under deterministic dynamics (as a method of choice for phase space sampling), can be expected to be more powerful than standard equilibrium methods simply because Crooks' and Jarzynski's identity hold under very general conditions on the dynamical process (i.e., time reversibility and phase space conservation), including completely artificial processes. For example, a molecular dynamics (MD) simulation with a symplectic integrator (like the Verlet algorithm) will give essentially exact free energies for arbitrarily large step sizes even when the energy might not be well preserved.[21] In contrast, since an equilibrium computation relies on the more restrictive condition of enforcing the canonical distribution, the integration time step must have a typical standard size. In other words, the nonequilibrium approach requires an equilibrium sampling only at $t = 0$ whereas equilibrium methods require canonical equilibrium at all times in the simulation. Furthermore, the feature perhaps most striking of the aforementioned nonequilibrium methods is that irreversible work can be directly used for the calculation of free energies, in contrast with traditional nonequilibrium methods,[22] where irreversible work was employed to provide bounds on the relevant thermodynamic potential.

In MD simulations, it is often advantageous to use constraints. They allow us to focus the computational effort on the dynamics relevant to the time scale of the particular phenomena of interest. Rigid-body dynamics are a peculiar case of constrained dynamics where vibrational motions (typically much faster than the rotational and translational ones) are ignored. The recent development of symplectic integrators for rigid bodies[23] has provided the necessary tools for the application of nonequilibrium methods in systems with rigid models.

Rigid models have been extensively used in classical simulations of water, as well as in quantum simulations. The quantum-mechanical rigid-body treatment of water molecules was introduced decades ago by Rossky and co-workers[24,25] for the calculation of equilibrium properties of quantum liquid water, and has also been used previously for ionic water clusters.[26]

† Present address: Department of Chemistry, University of Illinois at Urbana−Champaign.

10.1021/jp908742n
Published on Web 04/08/2010

This approach is motivated by the fact that the water molecular mass, M, is relatively large whereas the molecular moments of inertia $(I_x, I_y, I_z) = \mathrm{diag}(\mathbf{I})$ are relatively small. It is worth noting that this approach has proven also useful for the calculation of dynamical properties of quantum water in the context of centroid molecular dynamics,[27–31] as well as the closely related ring polymer molecular dynamics method.[32,33] (For a recent review on quantum simulations of bulk water see ref 34.)

In this work, we investigate the relevance of protonic quantum effects on the free energy of dissociation (or formation) of the paradigm $I^-(H_2O)_5$ using Crook's fluctuation relation in the context of classical and quantum (path-integral) rigid water models. Quantum effects on the potential of mean force (PMF) of the paradigm $Na^+(H_2O)_{12}$ are also evaluated via a nonequilibrium *computational experiment*. The article is organized as follows. Section II gives an overview of the path-integral representation used in this work in the context of rigid-body dynamics. Sections III and IV present the nonequilibrium calculation of the dissociation free energy of the iodide-water cluster and of the PMF for the sodium-water cluster, respectively. Concluding remarks follow in section V.

II. Theoretical Background and Model System

A. Path-Integral Representation with Rigid Models. A brief overview of the path-integral approach with rigid bodies is presented in this section. We refer to a cluster with a single quantum water molecule for notational simplicity; the generalization to a system with n rigid molecules is straigtforward. The canonical partition function of the system can be written in (discretized) path-integral form as[24,25]

$$Z = \frac{(mM)^{3/2}}{(2\pi\beta\hbar^2)^3}\int \mathrm{d}\mathbf{r}\int \mathrm{d}\mathbf{R}\,\rho(\mathbf{r},R) \tag{1}$$

where

$$\rho(\mathbf{r},\mathbf{R}) \approx \left(\frac{P}{2\pi\beta\hbar^2}\right)^{3P/2}\left[\prod_{k=1}^{P} I_k^{3/2}\int \mathrm{d}\mathbf{\Omega}_k\right]\times \exp[-\beta\Phi(\mathbf{r},\mathbf{R},\mathbf{\Lambda})] \tag{2}$$

and

$$\Phi(\mathbf{r},\mathbf{R},\mathbf{\Lambda}) = \sum_{k=1}^{P}\left[\frac{I_k P}{2\beta^2\hbar^2}\Theta^2(\mathbf{\Omega}_k,\mathbf{\Omega}_{k+1}) + \frac{1}{P}U(\mathbf{r},\mathbf{R},\mathbf{\Omega}_k)\right] \tag{3}$$

In these equations, $\beta = 1/kT$, P is the number of (discrete) beads, and $\mathbf{r}$ and $\mathbf{R}$ represent the ion and water molecular center-of-mass coordinates, respectively. The discrete configuration of the molecular orientational path is denoted by $\mathbf{\Lambda} \equiv (\mathbf{\Omega}_1,...,\mathbf{\Omega}_P)$. In eq 3, $\mathbf{\Omega}_{P+1} = \mathbf{\Omega}_1$, $\Theta(\mathbf{\Omega}_k,\mathbf{\Omega}_{k+1})$ is the rotation angle between orientations k and $k+1$, and I_k is the moment of inertia associated with that rotation. Note that the classical limit is found by setting $P = 1$ and $I_k = (I_xI_yI_z)^{1/3}$.

Although the path-integral in eq 2 can be evaluated with Monte Carlo methods (as in path-integral Monte Carlo or PIMC[24]), the focus here will be on the use of molecular dynamics, often referred to as path-integral molecular dynamics (PIMD).[25,35] In this approach, the dynamics is generated by adding an initial kinetic energy,

$$K_I = \frac{\mathbf{p}^2}{2m} \tag{4}$$

$$K_M = \frac{\mathbf{P}^2}{2M} \tag{5}$$

$$K_{\mathrm{rot}} = \sum_{k=1}^{P}\left(\frac{{L_{x,k}}^2}{2I'_x} + \frac{{L_{y,k}}^2}{2I'_y} + \frac{{L_{z,k}}^2}{2I'_z}\right) \tag{6}$$

to the ion and molecular translational and rotational motions. In eqs 4−6, $\mathbf{p} = \dot{\mathbf{r}}/\mathbf{m}$, $\mathbf{P} = \dot{\mathbf{R}}/M$ and $\mathbf{L}_k = \mathbf{I}'\cdot\mathbf{w}_k$. Note that the moments of inertia $(I'_x, I'_y, I'_z) = \mathrm{diag}(\mathbf{I}')$ need not be equal to those of the water molecule and can be chosen to perform an efficient dynamical sampling. Equation 1 can then be written as a phase space integral, i.e.

$$Z = \left(\frac{1}{2\pi\hbar}\right)^6\left(\frac{P}{2\pi\beta\hbar^2}\right)^{3P/2}\int \mathrm{d}\mathbf{r}\int \mathrm{d}\mathbf{p}\int \mathrm{d}\mathbf{R}\int \mathrm{d}\mathbf{P}\times \left[\prod_{k=1}^{P}\left(\frac{I_k\beta}{2\pi\tilde{I}}\right)^{3/2}\int \mathrm{d}\mathbf{\Omega}_k\int \mathrm{d}\mathscr{Y}_k\right]\exp[-\beta\mathscr{H}] \tag{7}$$

where

$$\mathscr{H} = K_I + K_M + K_{\mathrm{rot}} + \Phi \tag{8}$$

with $\tilde{I} = (I'_xI'_yI'_z)^{1/3}$ and Φ is defined in eq 3. In eq 7, $\mathscr{Y}_k$ is the conjugate momentum of the orientational variable $\mathbf{\Omega}_k$.

The Hamiltonian of eq 8 provides the basis for the PIMD algorithm. Note that while the translational kinetic terms appearing in eqs 7 and 8 are embodied in the prefactor of eq 1, the rotational kinetic term has been introduced to generate an artificial dynamics on the P orientations. This fictitious rotational dynamics allows the PIMD evaluation of the discrete path-integral in eq 2, whereas the full dynamics can be used to evaluate eq 1. The equations of motion derived from this Hamiltonian must be coupled to a canonical thermostating scheme to perform the $e^{-\beta\mathscr{H}}$ sampling of eq 7, such as the Nosé−Hoover[36,37] or Nosé−Hoover chain thermostat.[38]

The equations of motion are given by

$$\begin{aligned}\dot{\mathbf{p}} &= \mathbf{f}\\ \dot{\mathbf{P}} &= \mathbf{F}\\ \dot{\mathbf{L}}_k &= \mathbf{T}_k \qquad \text{for} \qquad k = 1, ..., P\end{aligned} \tag{9}$$

where the first two equations are the ion and molecular center of mass translational equations of motion with

$$\begin{aligned}\mathbf{f} &= \frac{-1}{P}\sum_{k=1}^{P}\nabla_{\mathbf{r}}U\\ \mathbf{F} &= \frac{-1}{P}\sum_{k=1}^{P}\nabla_{\mathbf{R}}U = \sum_{k=1}^{P}\mathbf{F}_k\end{aligned} \tag{10}$$

The force acting on the center of mass of bead k, $\mathbf{F}_k$, derives from the forces acting on the water interaction sites, i.e., $\mathbf{F}_k = \Sigma_\alpha\mathbf{F}_{k\alpha}$. The torques in eq 9 can be written as

$$\mathbf{T}_k = \boldsymbol{\tau}_k + \sum_{\alpha} (\mathbf{r}_\alpha - \mathbf{R}) \times \mathbf{F}_{k\alpha} \tag{11}$$

where $\boldsymbol{\tau}_k$ is a quantum contribution to the torque due to the harmonic term[39] [see eq 3] and $\mathbf{r}_\alpha$ is the position of the interaction site α in the laboratory axis frame.

B. Model System. The systems investigated in this work are composed of an ion (iodide or sodium) and (5 or 12) clustered water molecules. In all simulations, the ion is treated classically while the water molecules are treated either classically or quantum-mechanically as rigid bodies.

The potential $U(\mathbf{r},\mathbf{R},\boldsymbol{\Omega})$ in eq 3 includes the ion−water and water−water interactions. The ion−water potential is composed of a Lennard-Jones potential, $\mathcal{U}^{\mathrm{LJ}}$; an electrostatic point-charge contribution, $\mathcal{U}^{\mathrm{ch}}$; and a polarizability term, $\mathcal{U}^{\mathrm{pol}}$. The water model is defined similarly, with a Lennard-Jones and polarizability site on the water oxygen and a charge distribution on the atomic sites.[2]

The classical Hamiltonian of the ion−water cluster system is given by

$$H = \mathcal{K} + U(\mathbf{r},\mathbf{R}_1,...,\boldsymbol{R}_n,\boldsymbol{\Omega}_1,...,\boldsymbol{\Omega}_n) = \mathcal{K} + \sum_{i<j} [\mathcal{U}_{ij}^{\mathrm{pol}} + \mathcal{U}_{ij}^{\mathrm{ch}} + \mathcal{U}_{ij}^{\mathrm{LJ}}] + \sum_{i=1}^{n} [\mathcal{U}_i^{\mathrm{pol}} + \mathcal{U}_i^{\mathrm{ch}} + \mathcal{U}_i^{\mathrm{LJ}}] \tag{12}$$

where $\mathcal{K}$ is the total kinetic energy of the system, the second term represents the interaction between water molecules, and the third term reffers to the interaction between each water molecule and the ion. The water potential has been previously optimized for cluster simulations[2] and used in previous classical studies of ion−water clusters.[3,40] The convergence with P has been studied in quantum simulations[41] and $P = 5$ appears to be a reasonable choice. The thermostated dynamics is carried out with $1 + n + nP$ independent Nosé−Hoover chain thermostats of length 2; one coupled with the ion momentum, n coupled with the molecular translational motion and one coupled with each bead of the molecular rotational motion. The beads moments of inertia were set to be equal to the actual moments of inertia of the water molecule [i.e., $(I'_x, I'_y, I'_z) = (I_x, I_y, I_z)$]. The ion−water cluster system is confined by a hard-wall boundary with a spherical shape that defines the overall volume.

III. Dissociation/Formation Free Energy

This section presents the calculation of the dissociation/formation free energy, ΔF, of the $I^-(H_2O)_5$ cluster shown in Figure 1 to assess the relevance of protonic quantum effects. The simulation method and details are presented first, followed by a discussion of the results.

A. Computational Method. The calculation is based on the Crooks' fluctuation relation,[7,8] which relates the probability of work involved in dissociating the ion−water cluster (forward process) with the probability of the negative of the work involved in forming the ion−water cluster (reverse process) according to

$$\frac{P_{\mathrm{f}}(W)}{P_{\mathrm{r}}(-W)} \mathrm{e}^{-\beta W} = \mathrm{e}^{-\beta \Delta F} \tag{13}$$

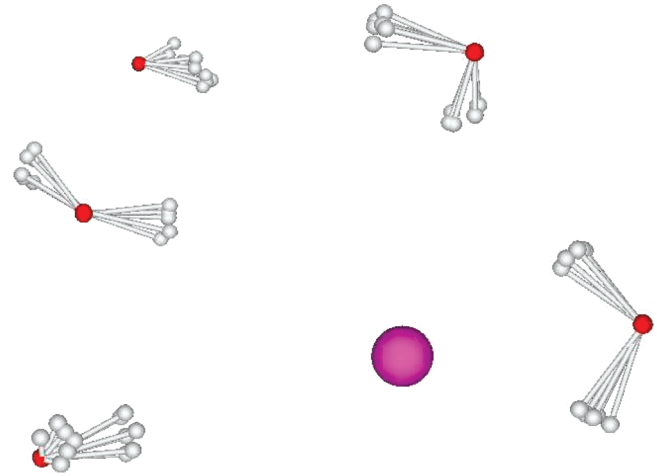

Figure 1. Snapshot of the $I^-(H_2O)_5$ cluster in the quantum simulations. The molecules are treated as rigid objects in the path-integral representation.

The intersection point of the aforementioned probabilities occurs at the value of the work at which it equals the dissociation free energy difference.

For the classical system, the interaction energy is written in the form

$$\mathcal{U}(\lambda_1,\lambda_2,\lambda_3) = U(\mathbf{r},\mathbf{R}_1,...,\mathbf{R}_n,\boldsymbol{\Omega}_1,...,\boldsymbol{\Omega}_n) - \sum_{i=1}^{n} [\lambda_1 \mathcal{U}_i^{\mathrm{pol}} + \lambda_2 \mathcal{U}_i^{\mathrm{ch}} + \lambda_3 \mathcal{U}_i^{\mathrm{LJ}}], \tag{14}$$

where U is defined by eq 12 and the second term effectively anihilates the ion as the parameters λ_1, λ_2, and λ_3 vary from zero to one. Indeed, $\mathcal{U}(0,0,0) = \mathcal{U}_0$ is the energy of the initial bounded cluster state and $\mathcal{U}(1,1,1) = \mathcal{U}_1$ is that of the final dissociated cluster state.

The time-dependent Hamiltonian for the nonequilibrium process is

$$\mathcal{H}(t) = \mathcal{H}(\lambda_1,\lambda_2,\lambda_3) = \mathcal{K} + \mathcal{U}(\lambda_1,\lambda_2,\lambda_3) \tag{15}$$

where the parameters λ contain the explicit time dependence. For the forward (reverse) process, the ion−cluster interactions are switched off (on) linearly with time. The time involved in the whole process is $t_{\mathrm{p}} = t_1 + t_2 + t_3$, with a protocol given by

$$\lambda_1(t) = \begin{cases} t/t_1 & \text{if} \quad t \le t_1 \\ 1 & \text{if} \quad t > t_1 \end{cases}$$

$$\lambda_2(t) = \begin{cases} 0 & \text{if} \quad t < t_1 \\ (t - t_1)/t_2 & \text{if} \quad t_1 \le t \le t_1 + t_2 \\ 1 & \text{if} \quad t > t_1 + t_2 \end{cases}$$

$$\lambda_3(t) = \begin{cases} 0 & \text{if} \quad t < t_1 + t_2 \\ (t - t_1 - t_2)/t_3 & \text{if} \quad t_1 + t_2 \le t \le t_p \end{cases} \tag{16}$$

The work probability for the forward process,

$$P_{\mathrm{f}}(W) = \langle \delta(W - W') \mathrm{e}^{-\beta W'} \rangle \tag{17}$$

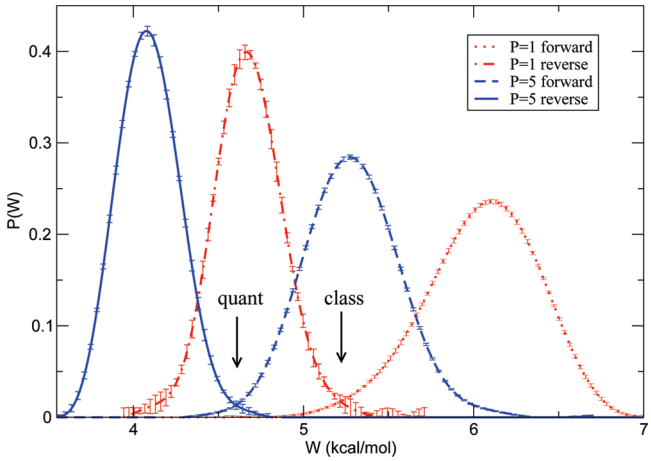

Figure 2. Forward and backward work distributions in analytical expanded form obtained with a Chevyshev smoothing process for the classical ($P = 1$) and quantum ($P = 5$) systems. The arrows indicate the intersection point of the forward and reverse work distributions.

was computed from Hamiltonian dynamics simulations, for which $W(t) = \mathcal{H}(t) - \mathcal{H}(0)$. The brakets $\langle\ \rangle$ in eq 17 indicate an average over canonically distributed initial conditions, and $\delta(x)$ is the Dirac Delta function. The initial conditions were generated in independent runs using Nosé−Hoover dynamics at $T = 125$ K, with $\lambda_1 = \lambda_2 = \lambda_3 = 0$ for the forward process and $\lambda_1 = \lambda_2 = \lambda_3 = 1$ for the reverse realizations. The reverse nonequilibrium process is carried out in a similar fashion by switching t to $t_p - t$. The quantum simulations are treated analogously to the classical ones using the quantum-classical isomorphism described in section IIA.

The equations of motion were integrated with a Verlet algorithm for rigid systems[23] with a time step of 2 fs and a spherical simulation box with a radius of 6 Å. Converged result were obtained with a total irreversible process of 20 ps, with $t_1 = 2$ ps, $t_2 = 14$ ps, and $t_3 = 4$ ps, and data collection over 2×10^4 realizations of the nonequilibrium process.

The work probabilities were obtained in analytical form via the corresponding derivative of the cumulative distribution of the values, which were independently obtained from the fitting to a Chevyshev polynomial or a Fourier expansion.[19,42] This process produces an essentially parameter-free result and significantly smooths out the resulting probability distributions in comparison with the conventional histogram data management. The smoothing process also provides sound error estimates by iteratively repeating the fitting procedure, while ignoring a fraction of the data points, which allows the estimation of local errors in the function.[19−42]

B. Results and Discussion. The work distributions obtained for the forward and reverse processes, $P_f(W)$ and $P_r(-W)$, for the classical ($P = 1$) and quantum ($P = 5$) systems are presented in Figure 2. The distributions are shifted toward lower values of work for the quantum system in comparison with the classical one. The dissociation free energy difference (i.e., the value of work at the intersection), is lower for the quantum system which implies that, not surprinsingly, the quantum cluster is more likely to release the ion. This result is clearly in agreement with expectactions. Due to proton delocalization, the atractive interactions between the quantum cluster and the ion are weaker than in the classical situation. The quantum free energy is also lowered by the cluster zero-point energy, in contrast to the classical picture.

The values of ΔF obtained for the classical system ($P = 1$) and the quantum systems with $P = 4$ and $P = 5$ using the two smoothing methods are listed in Table 1. Comparison of the quantum results at different values of the discretization parameter P demonstrates the numerical convergence of the quantum calculation, as the difference is of the order of the estimated errors. In relative terms, quantum effects reduce the dissociation free energy by 11% and are therefore significant. Both smoothing procedures yield essentially the same results since the difference lies well within the statistical uncertainties. As can be seen from Figure 2, the free energy differences were obtained from relatively small values of the work probabilities; however, the resulting error bar is about 1% of the reported quantum effect. The low value of the error bars is largely due to the robust handling of the collected data through the fitting process. The estimated errors of the quantum system are lower than in the classical situation, presumably because the sampling of the phase space is more efficient, since interactions are weaker in the quantum system.

TABLE 1: Dissociation Free Energies for Classical and Quantum $I^-(H_2O)_5$ at $T = 125$ K

	smoothing method	ΔF (kcal/mol)
classical	Fourier	5.18 ± 0.04
($P = 1$)	Chebyshev	5.22 ± 0.02
quantum	Fourier	4.66 ± 0.03
$P = 4$	Chebyshev	4.66 ± 0.03
quantum	Fourier	4.60 ± 0.02
$P = 5$	Chebyshev	4.60 ± 0.01

Finally, we note that the protocol employed here could be optimized at the expense of the parameters t_1, t_2, and t_3 such that the intersection point occurs at larger probability values. Furthermore, alternative protocols for the dynamical process are also possible, but one should note that certain choices might lead to nonstable dynamics; for example, turning off the Lennard-Jones interactions before the electrostic interactions invariably leads to unstable dynamics as atractives charges tend to get arbitrarily close and energy changes become dramatically large.

IV. Potential of Mean Force

This section presents the computation of the potential of mean force of the $Na^+(H_2O)_{10}$ cluster through a pulling-type nonequilibrium (hypothetical) *experiment* (Figure 3).

A. Computational Method. The time-dependent Hamiltonian used for the nonequilibrium process is given by

$$\mathcal{H}(t) = H + V_b(\xi,t) \tag{18}$$

where H is given by eq 12 and the biasing potential, V_b, is chosen to be

$$V_b(\xi,t) = \frac{k}{2}[\xi - \lambda(t)]^2 \tag{19}$$

In the equations above, ξ is the distance between the ion and the water cluster center of mass. A protocol linear with time is adopted for λ; $\lambda(t) = (t/t_p)\lambda_{max}$, for $0 \le t \le t_p$. In this context, the potential of mean force, $F(\xi)$, is then given by[9,11]

$$F(\xi) = -\frac{1}{\beta}\ln\langle\delta(\xi' - \xi)e^{-\beta\Xi(\xi')}\rangle + C \tag{20}$$

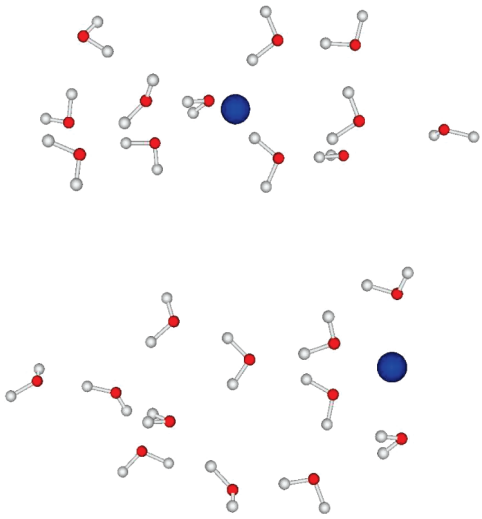

Figure 3. Snapshots of the irreversible dynamical process in the calculation of the clasical potential of mean force for $Na^+(H_2O)_{12}$. The top panel shows a sample of the initial configuration for the forward process ($\lambda = 0$), where the sodium ion is nearly at the cluster center of mass. The bottom panel shows a sample of a final configuration in the forward process ($\lambda = 5.5$ Å), where the sodium ion resides at the surface of the water cluster.

where the brakets $\langle\,\rangle$ represent an ensemble average over canonically distributed initial conditions according to the Hamiltonian $\mathscr{H}(0)$, $\Xi(\xi') = W - V_b(\xi',t)$ and C is an arbitrary constant.

The initial conditions were generated from Nosé−Hoover equilibrium simulations at $T = 200$ K, and the nonequilibrium process was also carried out using Nosé−Hoover dynamics. The work was then computed according to

$$\begin{aligned} W(t) &= \int_0^t \frac{\partial \mathscr{H}(t')}{\partial \lambda}\frac{\partial \lambda}{\partial t'}\,dt' \\ &= \frac{k\lambda_{max}}{t_p}\int_0^t [\lambda(t') - \xi]\,dt' \end{aligned} \tag{21}$$

For the dynamical process, the protocol time chosen is $t_p = 6$ ps as $\lambda(t)$ goes from 0 to $\lambda_{max} = 5.5$ Å. The integration time step used for the dynamical process is 3 fs, with a simulation box with a radius of 10 Å, and $k = 6.0$ kcal mol^{-1} Å^{-2}. Note that the reverse process, obtained from time inversion of the dynamics according to $t \rightarrow t_p - t$, provides an independent meassurement of the same function, $F(\xi)$, except for the arbitrary constant.

B. Results and Discussion. The potential of mean force for the classical and quantum systems obtained for the forward and reverse processes are shown in Figure 4. The classical (and the quantum) functions obtained from the forward and reverse processes look qualitatively similar, except for an arbitrary constant shift. The minimum in the potential of mean force occurs at shorter distances and is less pronounced for the quantum system than for the classical one. At large distances, the classical system exhibits a larger free energy barrier. These results are consistent with a weaker (attractive) interaction between the ion and the water molecules in the quantum case compared to the classical situation.

In spite of the smooth appearance of the potential of mean force, the local errors associated with the slow convergence of the exponential average in eq 20 are not negligible. This is a typical problem that arises with the Jarzyinski work relation as

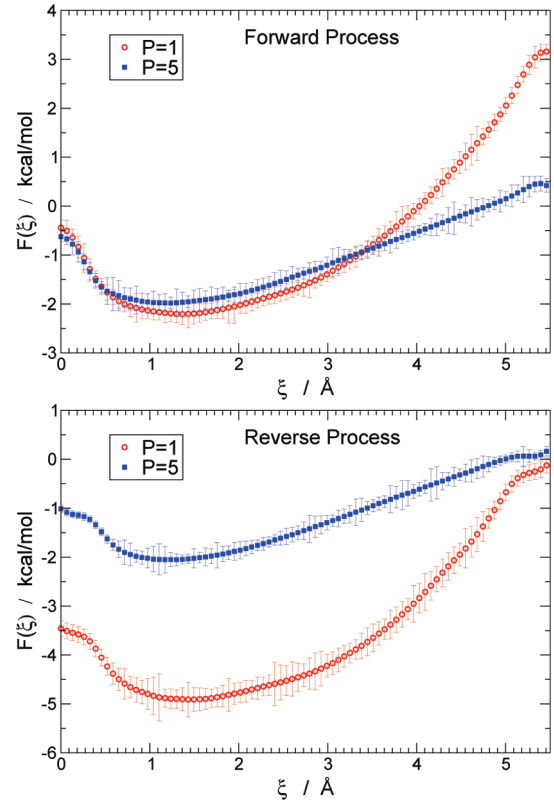

Figure 4. Classical ($P = 1$) and quantum ($P = 5$) potential of mean force $F(\xi)$ as a function of the distance between the ion and the cluster center of mass, calculated from the forward (top panel) and reverse (bottom panel) processes.

the average is dominated by fluctuations. In other words, the infrequent appeareance of small values of $\Xi(\xi)$ govern the average and significantly affect the convergence and estimation of the errors. There are, however, several ways to alleviate the significance of the statistical errors. The use of Nosé−Hoover dynamics for the time-dependent evolution, for example, enforces some level of thermal equilibration, and in the limit of a quasi-static process, this reduces to an equilibrium scheme equivalent to umbrella sampling. Note that such thermalization is absent when Hamiltonian dynamics is used and the quasi-static limiting process does not reduce to an equilibrium technique.

The potential of mean force is related to the radial probability distribution of the ion−cluster center-of-mass distance, $Pr(\xi)$, as

$$\Pr(\xi) \sim 4\pi\xi^2 e^{-\beta F(\xi)} \tag{22}$$

and the latter most conveniently expresses the physical information contained in the potential of mean force. This probability distribution is normalized for comparison purposes, i.e.

$$\int_0^{\lambda_{max}} \Pr(\xi)\,d\xi = 1 \tag{23}$$

Figure 5 shows the normalized ion−cluster center-of-mass probability distributions obtained for the classical and quantum systems from the forward and reverse processes. The distributions obtained from the forward and reverse processes are very similar, reflecting the aforementioned qualitative similarity of the potentials of mean force (cf. the top and bottom panels of

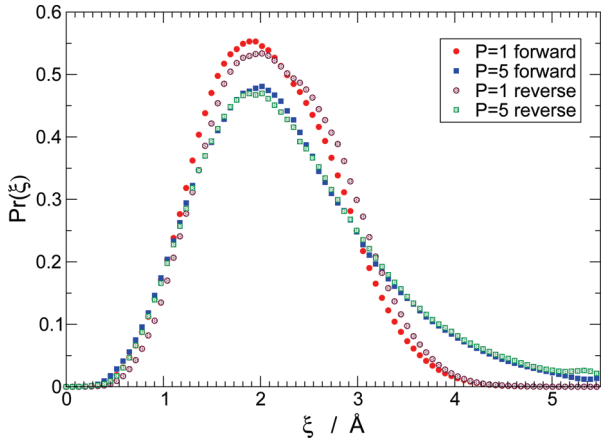

Figure 5. Probability distributions of the radial distance between the ion and the cluster center of mass for the classical and quantum systems calculated in the forward and reverse processes.

Figure 4). The quantum probability distributions are broader and peak at a lower value, compared to their classical counterpart. These structural differences between the classical and quantum systems provide a quantitative meassure of quantum effects in this system. Clearly, the delocalization and weakening of the attractive interactions in the quantum system cause a reduced ordering of the cluster structure and a higher propensity of the ion to *visit* the surface of the cluster (even though the sodium ion resides mostly in the interior of the cluster, $\xi \sim 2$ Å).

The discrepancies between the forward and reverse probability functions shown in Figure 5 are a quantitave measure of the bias introduced in the calculation of the potential of mean force by the nonequilibrium protocol used in the forward and reverse directions. It is clearly seen that while the chosen protocol is optimum for the quantum calculation, the classical values show sligthly larger errors. This can again be understood as a consequence of the fact that the stronger interactions (of the classical system) critically affect ergodicity in the statistical sampling. In general, however, it is possible to combine the forward and reverse probability distributions (or potentials of mean force) to produce a unique and more accurate estimation of the free energy profile. The Appendix discusses how to express the forward and reverse potentials of mean force with respect to the same free energy state, which makes them directly comparable, without resorting to an independent computation of the free energy difference associated to the initial and final biased states.

Finally, it is worth noting that the dynamical process employed in this study induces, by design, a separation between the ion and the cluster center of mass by acting on every particle of the system. Thus, although the overall scheme might resemble certain experimental settings regarding single-molecule manipulations, direct identification with a real experiment should be cautious (at the very least). For example, the total forces and torques in the system are manifestly zero in the simulation; however, that might be difficult to achieve in a particular experiment. It is also worth mentioning that in the quantum case the time variable has no rigorous connection to real time, so the irreversible process is fictitious. In fact, the real-time quantum dynamics of this system is obviously quite complex.

V. Conclusions

In this work, the relevance of protonic quantum effects in the free energy of ion−water systems has been assessed by employing nonequilibrium simulation methods, combined with rigid-body path-integral techniques. The use of rigid water models is advantageous for two main reasons; the integration time step can be large (in comparison with that used for flexible models), and the discretized path-integral converges with a much lower number of beads. A recently developed symplectic integrator for rigid bodies is used to carry out an accurate implementation of the Crooks fluctuation relation and the Jarzynsky work relation for the computation of free energies and potentials of mean force.

The dissociation free energy of the paradigm $I^-(H_2O)_5$ was shown to be reduced by 11% due to quantum effects, which is significant. The use of a rigorous smoothing procedure for the computation of the work probability distribution significantly enhances the applicability of the Crooks fluctuation theorem to realistic systems. It is important to emphasize that the quantum calculation is possible due to the convergence of the work distribution with the discretization parameter P (introduced in the path-integral representation), a convergence that has been previously analyzed analytically and numerically for model systems.[19,20] Quantum effects on the potential of mean force of $Na^+(H_2O)_{12}$ as a function of the ion−cluster center-of-mass distance were also found to be important. Overall, the results suggest that quantization should play a significant role in the structure of ion−water clusters, the thermodynamics of ion solvation and the kinetics of ion transport in aqueous environments.

Acknowledgment. This work was supported by the Natural Sciences and Engineering Research Council (NSERC) of Canada. Computational resources were provided by the Reseau Quebecois de Calcul Haute Performance (RQCHP). LHdlP wishes to acknowledge grant No. CHE 08-09699 from the US National Science Foundation awarded to Prof. Makri for support of his postdoctoral stay at UIUC, during which this work was completed.

Appendix A

Since the practical utility of nonequilibrium methods relies on the notoriosly challenging convergence of exponential averages, several estrategies have been proposed in the literature to alleviate this problem.[11,43–45] This Appendix presents still another method that allows us to estimate a more accurate potential of mean force (PMF) by combining the data obtained from the forward and reverse processes. It is motivated by the fact (already noted in the main text) that all the relevant physical information stored in the potential mean force can be obtained from the associated probability distribution which, for the purpose of comparison, is often normalized.

The PMF is defined as

$$F(\xi) = -\frac{1}{\beta}\ln\langle\delta(\xi' - \xi)\rangle \tag{A1}$$

where the brakets indicate an ensemble average over the system Hamiltonian H. For the irreversible process in the forward and reverse directions described in section IV, eq 20 becomes

$$\begin{aligned} F_{\text{for}}(\xi) &= F(\xi) + F - \mathscr{T}_0 \\ F_{\text{rev}}(\xi) &= F(\xi) + F - \mathscr{T}_{\lambda_{\max}} \end{aligned} \tag{A2}$$

where the constants have been explicitly indentified: F is the system free energy, and $\mathscr{T}_0$ and $\mathscr{T}_{\lambda_{\max}}$ are the free energies of

the biased system with V_b fixed at $\lambda = 0$ and $\lambda = \lambda_{max}$, respectively. [In contrast to the notation used in section IV, we distinguish here between $F_{for}(\xi)$, $F_{rev}(\xi)$ and $F(\xi)$.]

Therefore, the difference between the forward and reverse PMFs is given by the free energy difference $\Delta\mathscr{F} = \mathscr{F}_{\lambda_{max}} - \mathscr{F}_0$. Since this free energy difference can be independently estimated (from equilibrium or nonequilibrium simulations), it is possible to express the PMF computed in one direction as a function of the PMF computed in the reverse direction. This is indeed the path followed or suggested by several authors.[11,43–45]

An alternative to this approach is to construct two new forward and reverse PMFs anchored to the same reference state. For the forward process, we propose the estimator

$$F'_{for}(\xi) = F_{for}(\xi) - C'_{for} \tag{A3}$$

with

$$C'_{for} = -\frac{1}{\beta}\ln\left[\int_0^{\lambda} e^{-\beta F_{for}(\xi)}\, d\boldsymbol{\xi}\right] \tag{A4}$$

In eq A4, λ can be chosen to be as large as permitted by the available volume (i.e., $0 < \lambda \leq \mathscr{R}$), and ξ is, for example, the vector distance between the ion and the center of mass of the cluster. An analogous estimator, $F'_{rev}(\xi)$, can be constructed for the reverse process.

Then, we note that

$$\begin{aligned} e^{-\beta[F'_{for}(\xi) - F'_{rev}(\xi)]} &= e^{-\beta\Delta\mathscr{F}} e^{-\beta(C'_{rev} - C'_{for})} \\ &= e^{-\beta\Delta\mathscr{F}} \frac{\int_0^{\lambda} e^{-\beta F_{rev}(\xi)}\, d\boldsymbol{\xi}}{\int_0^{\lambda} e^{-\beta F_{for}(\xi)}\, d\boldsymbol{\xi}} \\ &= e^{-\beta\Delta\mathscr{F}} \frac{e^{-\beta(F - \mathscr{F}_{\lambda_{max}})} \int_0^{\lambda} e^{-\beta F(\xi)}\, d\boldsymbol{\xi}}{e^{-\beta(F - \mathscr{F}_0)} \int_0^{\lambda} e^{-\beta F(\xi)}\, d\boldsymbol{\xi}} \\ &= 1 \end{aligned} \tag{A5}$$

which shows that the functions $F'_{for}(\xi)$ and $F'_{rev}(\xi)$ are conceptually identical. Thus, it is not imperative to carry out a third measurement (namely, an independent calculation of $\Delta\mathscr{F}$) to relate the PMFs obtained from the forward and reverse processes.

There are, however, statistical differences associated to independent measurements in practice. The above scheme can be used to optimize the forward and reverse nonequilibrium protocols by verifying that, for example, the criteria $F'_{for}(\xi) \approx F'_{rev}(\xi)$ is satisfied. Alternatively, an independent calculation of $\Delta\mathscr{F}$ can be used as an indicator of the numerical convergence while the criteria $C'_{for} - C'_{rev} \approx \Delta\mathscr{F}$ is used. Since the nonequilibrium process is carried out in the interval $0 \leq \lambda \leq \lambda_{max}$, the natural choice in eq A4 is $\lambda = \lambda_{max}$. In this way, all the information available from each of the forward and reverse PMFs is used in the corresponding estimates.

Furthermore, the interpretation of the constants C'_{for} and C'_{rev} is straightforward. For example, by choosing $\lambda = \mathscr{R}$ in eq A4, we can write

$$\begin{aligned} \int_0^{\mathscr{R}} e^{-\beta F'_{for}(\xi)}\, d\boldsymbol{\xi} &= e^{\beta C'_{for}} \int_0^{\mathscr{R}} e^{-\beta F_{for}(\xi)}\, d\boldsymbol{\xi} \\ &= 1 \end{aligned} \tag{A6}$$

which shows, formally, that $F'_{for}(\xi) = F'_{rev}(\xi) = F(\xi)$. Hence, for this case, the constants represent the following free energy differences:

$$\begin{aligned} C'_{for} &= F - \mathscr{F}_0 \\ C'_{rev} &= F - \mathscr{F}_{\lambda_{max}} \end{aligned} \tag{A7}$$

In general, however,

$$\begin{aligned} C'_{for} &= \tilde{F} - \mathscr{F}_0 \\ C'_{rev} &= \tilde{F} - \mathscr{F}_{\lambda_{max}} \end{aligned} \tag{A8}$$

where $\tilde{F}$ is the free energy associated to the system under the restriction that the distance between the ion and the center of mass is bounded by $0 \leq \xi \leq \lambda$, i.e.

$$\tilde{F} = F - \frac{1}{\beta}\ln\left[\int_0^{\lambda} e^{-\beta F(\xi)}\, d\boldsymbol{\xi}\right] \tag{A9}$$

References and Notes

(1) Topol, I. A.; Tawa, G. J.; Burt, S. K.; Rashin, A. A. *J. Chem. Phys.* **1999**, *111*, 10998.
(2) Peslherbe, G. H.; Ladanyi, B. M.; Hynes, J. T. *Chem. Phys.* **2000**, *258*, 201.
(3) Koch, D.; Peslherbe, G. H. *Chem. Phys. Lett.* **2002**, *359*, 381.
(4) Merchant, S.; Asthagiri, D. *J. Chem. Phys.* **2009**, *130*, 195102.
(5) Jarzynski, C. *Phys. Rev. Lett.* **1997**, *78*, 2690.
(6) Jarzynski, C. *Phys. Rev. E* **1997**, *56*, 5018.
(7) Crooks, G. E. *J. Stat. Phys.* **1998**, *90*, 1481.
(8) Crooks, G. E. *Phys. Rev. E* **1999**, *60*, 2721.
(9) Hummer, G.; Szabo, A. *Proc. Natl. Acad. Sci. U.S.A.* **2001**, *98*, 3658.
(10) Jarzynski, C. *Proc. Natl. Acad. Sci. U.S.A.* **2001**, *98*, 3636.
(11) Paramore, S.; Ayton, G. S.; Voth, G. A. *J. Chem. Phys.* **2007**, *126*, 051102.
(12) Mukamel, S. *Phys. Rev. Lett.* **2003**, *90*, 170604.
(13) Esposito, M.; Mukamel, S. *Phys. Rev. E* **2006**, *73*, 046129.
(14) Roeck, W. D.; Maes, C. *Phys. Rev. E* **2004**, *69*, 026115.
(15) Talkner, P.; Hänggi, P. *J. Phys. A, Math. Gen.* **2007**, *40*.
(16) Talkner, P.; Lutz, E.; Hänggi, P. *Phys. Rev. E* **2007**, *75*, 050102(R).
(17) Talkner, P. Hänggi, P. Morillo, M. A microcanonical quantum fluctuation theorem (2007), arXiv:0707.2307v1 [cond-mat.stat-mech].
(18) Deffner, S.; Lutz, E. *Phys. Rev. E* **2008**, *77*, 021128.
(19) van Zon, R.; Hernández, L.; Peslherbe, G. H.; Schofield, J. *Phys. Rev. E* **2008**, *78*, 041103.
(20) van Zon, R.; Hernández, L.; Peslherbe, G. H.; Schofield, J. *Phys. Rev. E* **2008**, *78*, 041104.
(21) Lechner, W.; Oberhofer, H.; Dellago, C.; Geissler, P. *J. Chem. Phys.* **2006**, *124*, 044113.
(22) Reinhardt, W. P.; Miller, M. A.; Amon, L. M. *Acc. Chem. Res.* **2001**, *35*, 607.
(23) van Zon, R.; Schofield, J. *Phys. Rev. E* **2007**, *75*, 056701.
(24) Kuharsky, R. A.; Rossky, P. J. *J. Chem. Phys.* **1985**, *82*, 5164.
(25) del Buono, G. S.; Rossky, P. J.; Schinitker, J. *J. Chem. Phys.* **1991**, *95*, 3728.
(26) Gai, H.; Schenter, G. K.; Dang, L. X.; Garrett, B. C. *J. Chem. Phys.* **1996**, *105*, 8835.
(27) Jang, S.; Voth, G. A. *J. Chem. Phys.* **1999**, *111*, 2357.
(28) Jang, S.; Voth, G. A. *J. Chem. Phys.* **1999**, *111*, 2371.
(29) Hernández de la Peña, L.; Kusalik, P. G. *J. Chem. Phys.* **2004**, *121*, 5992.
(30) Hernández de la Peña, L.; Kusalik, P. G. *J. Am. Chem. Soc.* **2005**, *127*, 5246.
(31) Hernández de la Peña, L.; Kusalik, P. G. *J. Chem. Phys.* **2006**, *125*, 074105.
(32) Craig, I. R.; Manolopoulos, D. E. *J. Chem. Phys.* **2004**, *121*, 3368.
(33) Miller, T. F., III.; Manolopoulos, D. E. *J. Chem. Phys.* **2005**, *123*, 154504.
(34) Paesani, F.; Voth, G. A. *J. Phys. Chem. B* **2009**, *113*, 5702.
(35) Parinello, M.; Rahman, A. *J. Chem. Phys.* **1983**, *80*, 860.
(36) Nosé, S. *J. Chem. Phys.* **1984**, *81*, 511.
(37) Hoover, W. G. *Phys. Rev. A* **1985**, *31*, 1695.

(38) Martyna, G. J.; Klein, M. L.; Tuckerman, M. *J. Chem. Phys.* **1992**, *97*, 2635.
(39) Hernández, L.; Kusalik, P. G. *Mol. Phys.* **2004**, *102*, 927.
(40) Koch, D. Hern L. ández de la Peña, L. Peslherbe G. H. Manuscript to be published.
(41) Hernández de la Peña, L. Koch, D. Peslherbe G. H. Manuscript to be published.
(42) Berg, B. A.; Harris, R. C. *Comput. Phys. Commun.* **2008**, *179*, 443.
(43) Minh, D. L. *Phys. Rev. E* **2006**, *74*, 061120.
(44) Minh, D. L.; Adib, A. B. *Phys. Rev. Lett.* **2008**, *100*, 180602.
(45) Chelli, R.; Procacci, P. *Phys. Chem. Chem. Phys.* **2009**, *11*, 1152.

JP908742N